JOURNAL OF PROPULSION AND POWER
Vol. 12, No. 1, January–February 1996

Internal Flowfield Characteristics of a Scramjet Inlet at Mach 10

D. M. Van Wie* and D. A. Ault†
Johns Hopkins University, Laurel, Maryland 20723

A combined experimental and analytical investigation has been conducted to study the internal flowfield characteristics of a two-dimensional scramjet inlet at Mach 10. The inlet under consideration is a mixed external/internal compression design that uses a two-dimensional forebody to turn the flow outward followed by a single cowl shock wave to turn the flow back toward the inlet centerline. A dominant feature of the inlet flowfield is the interaction between the cowl shock and the thick forebody boundary layer that is swallowed by the inlet. At the design operating condition, this interaction occurs near a shoulder where the cowl shock is nearly canceled. The ability of the inlet to operate for a range of cowl shock positions is demonstrated. Some information is also provided on the effects of Reynolds number, wall-to-freestream temperature ratio, nose radius, and cowl lip radius. A procedure is presented for relating the flow nonuniformity in the inlet throat to the wall pressure distribution in a constant area duct downstream of the inlet throat. Using this procedure, the extent to which the cowl shock can be canceled at the shoulder is shown to be a function of the thickness of the forebody boundary layer.

Nomenclature

C_h = Stanton number
h = throat height
L = length of cowl
M = Mach number
P = pressure
R = radius
Re = Reynolds number
T = temperature
X = axial coordinate
Y = vertical coordinate
δ = boundary-layer thickness
δ_f = final forebody angle
δ_i = initial forebody angle
η_{KE} = kinetic energy efficiency
$\eta_{KE\text{-}ad}$ = adiabatic kinetic energy efficiency
σ = standard deviation

Subscripts
av = average condition
b = innerbody
c = cowl
DES = design condition
e = boundary-layer edge property
ma = mass-averaged condition
n = forebody nose
sa = stream-thrust-averaged condition
w = wall condition
θ = boundary-layer momentum thickness
0 = freestream
4 = inlet throat

Introduction

THE inlet of a scramjet engine serves to capture and compress the engine airflow before the introduction of the fuel within the combustor. Previous studies of hypersonic inlet operating characteristics include investigations of two-dimensional, axisymmetric, and three-dimensional designs.[1–9] We can draw several important conclusions from these investigations.

1) Inlet performance can be sensitive to variations in geometric parameters such as nose and cowl lip bluntness.

2) Hypersonic inlets can be dominated by viscous effects, therefore, inlet performance can be sensitive to Reynolds number.

3) A control volume approach should be used for determining inlet performance.

4) Wall-cooling effects can be very important in determining the inlet operation.

In this article, we present the results of a combined experimental and analytical investigation of the operating characteristics of a two-dimensional class of hypersonic inlet. A schematic of the class of inlet under investigation is shown in Fig. 1. These mixed external/internal compression inlets contain a forebody, which turns the flow outward using a combination of a blunted wedge and isentropic turning. The forebody is characterized by a nose bluntness R_n, initial wedge angle δ_i, and final ramp angle δ_f. The forebody waves are designed to focus at the cowl lip at a prescribed freestream Mach number M_{DES}. A flat, horizontal cowl is used to generate a single cowl shock, which turns the flow back toward the inlet centerline. At a design operating condition, this cowl shock is canceled on an innerbody shoulder. The cowl is characterized by a cowl lip bluntness R_c and cowl lip coordinates (X_c, Y_c). The throat of the inlet is characterized by h. These inlets are considered two-dimensional designs because the primary flow character-

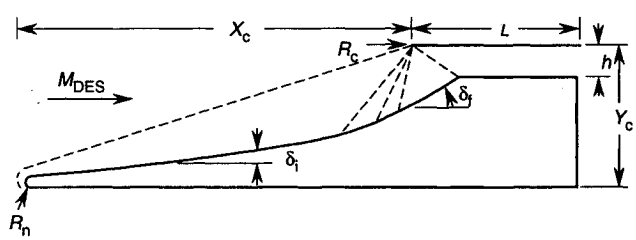

Fig. 1 Primary variables describing the class of inlet under investigation.

Received Feb. 2, 1994; presented as Paper 94-0584 at the AIAA 32nd Aerospace Sciences Meeting and Exhibit, Reno, NV, Jan. 10–13, 1995; revision received June 16, 1995; accepted for publication July 6, 1995.

*Principal Staff Engineer, Applied Physics Laboratory. Senior Member AIAA.

†Associate Staff Engineer, Applied Physics Laboratory. Member AIAA.

istics are designed using two-dimensional analysis. As is the case with all inlets of finite AR, three-dimensional features of the flowfield exist.

The goal in the development of any hypersonic inlet system is to define a geometry that provides an efficient compression process, generates low drag, produces nearly uniform flow entering the combustor, and provides these characteristics over a wide range of flight and engine operating conditions. The shock-on-shoulder operation of two-dimensional inlets offers the potential for meeting these design requirements. If the freedom exists to move the cowl in this particular class of inlet, a flexible design results that can accommodate changes in Mach number and angle of attack. For example, at any given Mach number and angle of attack, a cowl position can be found through horizontal and vertical translation that will produce the cowl shock-on-shoulder condition. Such a condition is considered desirable because inefficiencies associated with flow nonuniformity at the inlet throat are minimized and a relatively uniform flowfield is delivered to the combustor.

The primary issue associated with this class of inlet concerns the sensitivity of inlet operation to the position of the cowl shock relative to the innerbody shoulder. At off-design conditions, the cowl shock could potentially impinge on the innerbody either upstream or downstream of the shoulder. Under these circumstances, a large pressure gradient is imposed on the innerbody boundary layer, and boundary-layer separation may result. A combined experimental and analytical investigation of the operating characteristics of this class of inlet was undertaken to study the sensitivity of inlet operation to the cowl shock positioning. During this investigation, a limited amount of information was also acquired concerning the effects of Reynolds number, wall-to-freestream temperature ratio, and cowl lip bluntness.

The experimental portion of the program was conducted in the 48-in. shock tunnel at the Arvin/Calspan Advanced Research Center in Buffalo, New York. The tunnel uses a contoured nozzle with a replaceable nozzle throat to provide a range of freestream conditions. For this test series, the shock tunnel was operated such that total pressures up to 4600 psia and total temperatures up to 3300°R were achieved. The facility run time for all tests was in the range of 6–9 ms. All tests were conducted using nitrogen as the test medium.

The analytical portion of the investigation was conducted using computational fluid dynamics (CFD) codes developed by Science Applications International Corporation (SAIC).[10] These codes include a viscous shock-layer code for solution of the blunt forebody nose region, the SCRAMP parabolized Navier–Stokes (PNS) code for solution of the remaining external forebody flowfield, and the SCRINT PNS code for solution of the internal flowfield. All codes assume two-dimensional flow and use an upwind-differencing scheme. Because of the low temperatures encountered the inlet flowfields were generated assuming an ideal gas. The boundary layers can be either laminar, transitional, or fully turbulent. For the analysis presented herein, the onset location and length of transition were selected to provide the best agreement between the predicted and measured forebody heat transfer distributions. Turbulent flows were modeled with a two-equation k-ε model. For the external flowfield the computational grid contained 150 grid points in the vertical direction between the body and the bow shock and approximately 1600 points axially. For the internal flowfield the grid contained 150 points between the body and cowl and approximately 500 points axially. Between 20–32 points were maintained in the subsonic region of the boundary layers. Peak y^+ values for the first grid point off the wall were between 1.4–1.8 for all solutions, with values of y^+ generally maintained between 0.5–0.8.

Model Description

The inlet used as the focal point of this investigation was designed for Mach 20 operation at a dynamic pressure of 1000 lbf/ft^2. The inlet consists of a 5-deg initial forebody ramp followed by an isentropic compression region that turns the flow an additional 5 deg. The geometry of the inlet is provided later, with the origin of the (X, Y) coordinate system located at the theoretical sharp tip of the forebody. The widths of the external forebody and internal inlet are 23.0 and 3.0 in. wide, respectively. Note that the cowl lip is located at X = 35.9 in., and the innerbody shoulder is located at X = 40 in. Figure 2 is a photograph of the model.

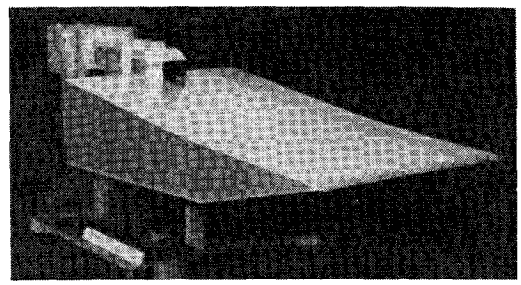

Fig. 2 Parametric inlet model used in test program.

$$
\begin{aligned}
&0 < X < 8.3566 && Y = (\tan 5\ \text{deg})X \\
&8.3566 < X < 23.3561 && Y = 9.8870 \times 10^{-5}(X - 8.3566)^3 \\
&&& \quad + 7.3687 \times 10^{-4}(X - 8.3566)^2 \\
&&& \quad + 0.08749(X - 8.3566) + 0.7311 \\
&23.3561 < X < 40.0 && Y = (\tan 10\ \text{deg})(X - 23.3566) + 2.54284 \\
&40.00 < X && Y = 5.4776
\end{aligned}
$$

The model was constructed such that the vertical position of the cowl Y_c, cowl lip radius R_c, and forebody nose leading-edge radius R_n, could be varied. The model was instrumented with pressure and heat transfer gauges to provide both measurements of the global performance of the inlet and diagnostic measurements, which were useful in understanding the operating characteristics of the inlet.

External Flowfield Results

A detailed description of the external flowfield results from this investigation are provided in Ref. 11. A few selected results are presented herein to provide the framework for understanding the internal operating characteristics of the inlet.

A typical schlieren photograph of the forebody flowfield in the vicinity of the cowl lip is shown in Fig. 3. The conditions corresponding to this photograph are M_0 = 10.4, Re = 5.7 × 10^6/ft, T_w/T_0 = 6.1, and R_n = 0.005 in. The forebody bow shock, isentropic compression field, and forebody boundary layer can be seen. Comparisons of the bow shock position and boundary-layer height between the PNS calculation and those measured from the schlieren photograph are shown in Fig. 4 on the Mach number profile obtained from the PNS calculation at the cowl lip plane. Good qualitative agreement between the analysis and test results are achieved for both the boundary-layer thickness and the bow shock position. Note that the PNS solution shows a boundary-layer thickness of approximately 0.5 in. and a core inviscid Mach number of 7.5.

Comparison of the calculated and measured pressure and heat transfer distributions over the external forebody at the same condition are shown in Fig. 5. In this figure the data are shown as discrete symbols and the results obtained from the CFD analysis are shown as solid lines. The errors bars on the test data represent the standard deviations in the measurements obtained over 10 runs conducted at this condition. In general, many factors affect measurement accuracy in addition to repeatability. Typically, the accuracy of pressure measurements in shock tunnels is approximately 5%, whereas the accuracy of heat transfer measurements is approximately 10%.

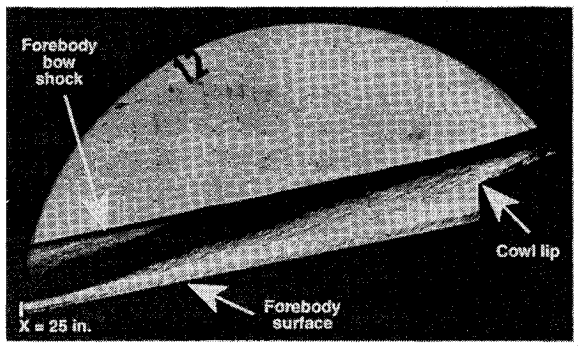

Fig. 3 Schlieren photograph of the forebody flowfield at M_0 = 10.4, Re = 5.7 × 10⁶/ft, T_w/T_0 = 6.1, and R_n = 0.005 in.

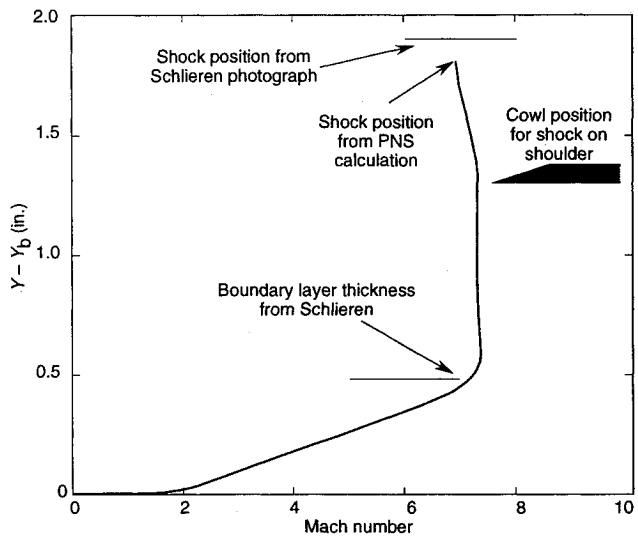

Fig. 4 Comparison of test results with PNS predictions in the plane of the cowl lip at M_0 = 10.4, Re = 5.7 × 10⁶/ft, T_w/T_0 = 6.1, and R_n = 0.005 in.

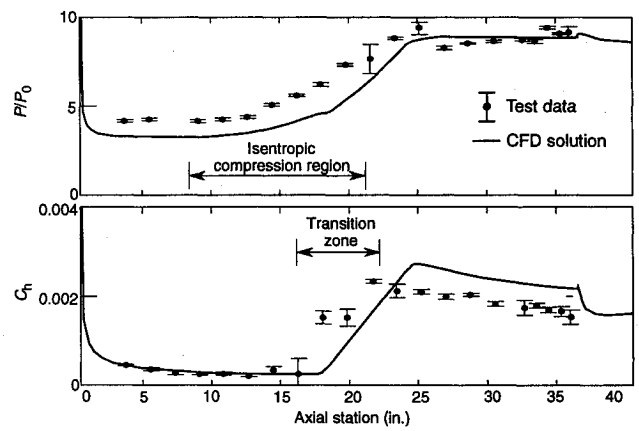

Fig. 5 Comparison of calculated and measured forebody pressure and Stanton number distributions at M_0 = 10.4, Re = 5.7 × 10⁶/ft, T_w/T_0 = 6.1, and R_n = 0.005 in.

As seen in the PNS results in Fig. 5, the pressure distribution consists of a nose region characterized by a rapidly decreasing pressure from the stagnation region, a pressure plateau corresponding to the flow over the first ramp, an isentropic compression region, and a final pressure plateau corresponding to the region downstream of the isentropic compression. The results indicate that the pressure on the first ramp was underpredicted by approximately 30%, whereas the pressure obtained after the isentropic compression shows good agreement between analysis and test result. In Ref. 11, the discrepancy between analysis and test was attributed to either a nonuniformity in the facility freestream or an underprediction of the inviscid/viscous coupling on the forward ramp.

The heat transfer distributions over the forebody shown in Fig. 5 consist of a laminar flow region followed by a region where the isentropic compression and transition are both present. Downstream of the isentropic compression, the boundary layer appears to be fully turbulent. The results show excellent agreement between the test data and calculations in the laminar region. Transition began at X = 17 in., where the PNS analysis indicated that Re_θ/M_e = 139. The results also show that the PNS analysis overpredicts the heat transfer in the turbulent region by approximately 20%. This difference between PNS analysis and test data might be improved with further refinement in the position and length of transition or improvements in the distribution of the PNS grid.

Internal Flow Results

Comparison of the test results and PNS calculations for the pressure distributions on the centerline of the cowl and innerbody surfaces are shown in Fig. 6 for a cowl vertical position (Y_c = 6.14 in.) near the shock-on-shoulder operating condition. This comparison is made for the baseline operation at M_0 = 10.4, Re = 5.7 × 10⁶/ft, and T_w/T_0 = 6.1, with R_n = 0.005 in. and R_c = 0.005 in. Reasonable agreement in the overall compression ratio was obtained, but the results show that the PNS calculation of the intersection of the cowl shock with the innerbody is approximately 0.5 in. downstream of that indicated by the data. This discrepancy between test data and analysis is thought to be caused by either the approximations within the PNS methodology, which prevent the upstream pressure influence, or by neglecting the cowl lip bluntness (R_c = 0.005 in.) in the calculations. Note that the agreement is fairly good for the overall inlet compression ratio between the measurements, which were taken on the model centerline, and the results from the two-dimensional PNS analysis. This observation implies that the internal flowfield structure is not dominated by three-dimensional aspects of the inlet geometry.

As previously stated, the primary uncertainty in the inlet operation concerned the sensitivity to the positioning of the cowl shock. This sensitivity was investigated by adjusting the cowl vertical height to position the cowl shock at various locations relative to the innerbody shoulder. This series of tests was conducted at M_0 = 10.4, Re = 5.7 × 10⁶/ft, and T_w/T_0 = 6.1, with R_n = 0.005 in. and R_c = 0.005 in. The vertical position of the cowl was varied between 6.34–5.69 in. With the inner-

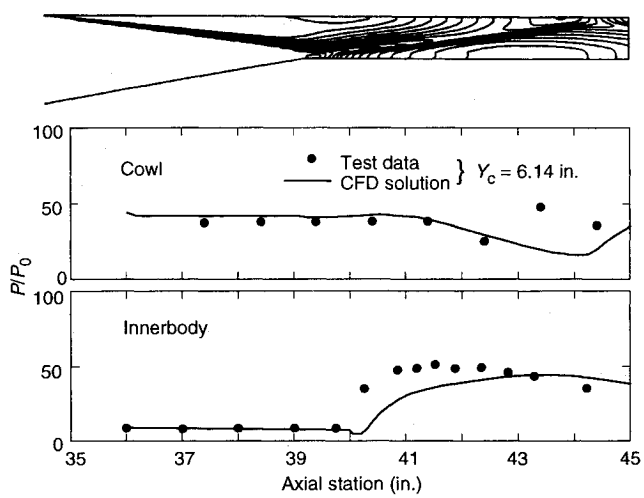

Fig. 6 Comparison of calculated and measured innerbody and cowl pressure distributions for operation near the shock-on-shoulder condition. (A flow-angle contour plot is also provided for reference.)

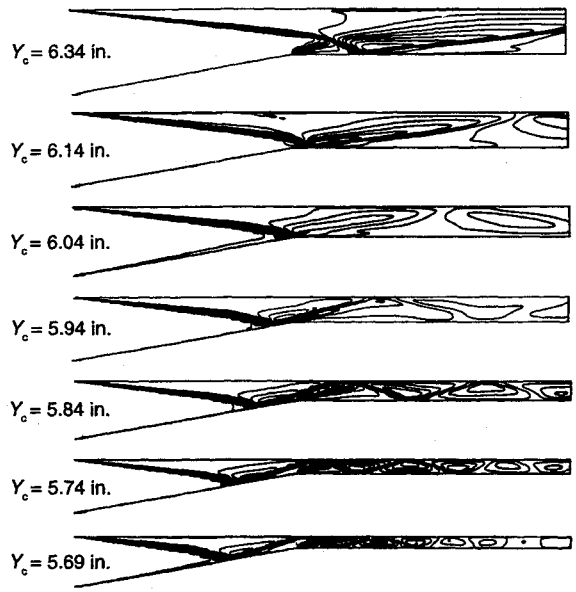

Fig. 7 Internal flow-angle contour plots showing the effect of cowl vertical position on the internal flow structure as predicted by PNS codes.

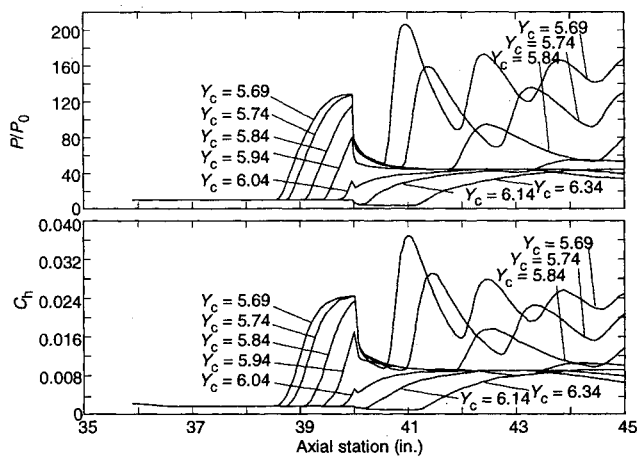

Fig. 8 PNS predictions of the effect of cowl position on innerbody wall pressure and heat transfer distributions.

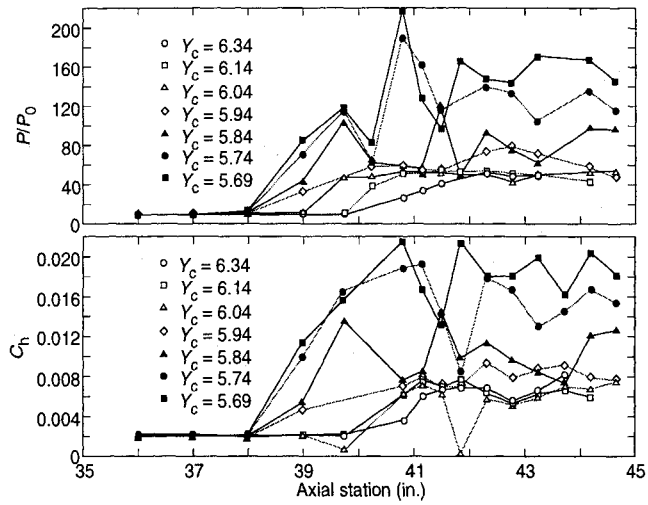

Fig. 9 Test results showing the effects of cowl position on innerbody wall pressure and heat transfer distributions.

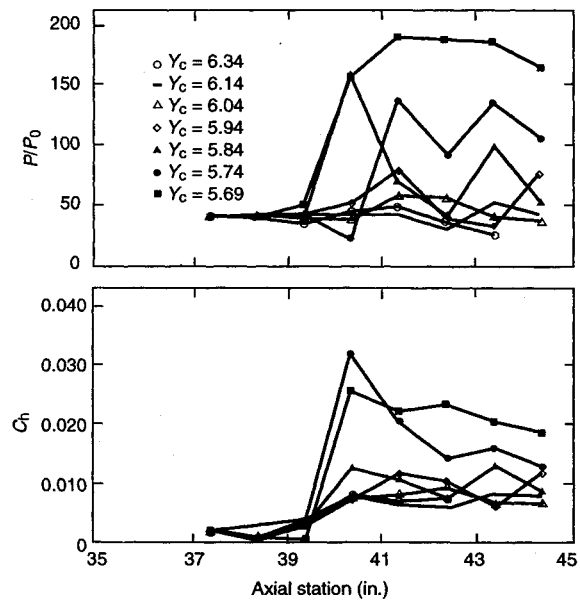

Fig. 10 Test results showing the effects of cowl position on cowl pressure and heat transfer distributions.

body shoulder height fixed at 5.478 in., a range of overall geometric contraction ratios between 7.35–26.79 and a range of internal contraction ratios between 1.84–4.40 were produced.

Contour plots of the flow angles within the internal portion of the inlet as calculated with the PNS code are shown in Fig. 7 for the cowl positions tested. The calculations show that the cowl shock intersects the innerbody downstream of the shoulder for the most open cowl position. As the cowl height is decreased, the location where the cowl shock intersects the innerbody moves forward. Near a cowl position of 6.04 in., the shock-on-shoulder condition is achieved. For cowl positions lower than this value, the cowl shock impinges forward of the shoulder. Physical constraints within the model limited testing near the second shock-on-shoulder condition where the cowl shock reflects from the innerbody and cowl before reimpinging on the innerbody near the shoulder. The lowest cowl position tested was 5.69 in., which resulted in a throat height of 0.212 in. At this cowl height, the cowl shock reflects from the innerbody and cowl prior to reimpinging on the innerbody just downstream of the shoulder.

The PNS results for the innerbody pressure and heat transfer distributions for the range of cowl positions tested are shown in Fig. 8. For $Y_c > 6.04$ in., the overexpansion of the flowfield around the shoulder and subsequent recompression are evident. For conditions with $Y_c < 6.04$ in., the flowfield overcompresses prior to the shoulder and re-expands around the shoulder.

The effects of the cowl position on the measured innerbody pressure and heat transfer distributions are shown in Fig. 9. The corresponding cowl pressure and heat transfer distributions are shown in Fig. 10. Qualitatively, many of the expected features of the flowfield are evident in the test data. For cowl positions near 6.0 in., the shock-on-shoulder condition was achieved with a relatively uniform pressure distribution in the constant area downstream of the shoulder. For $Y_c < 6.0$ in., the flow overcompresses and re-expands around the shoulder. For $Y_c > 6.0$ in., the overexpansion and recompression downstream of the shoulder are not seen. This discrepancy might be explained by the coarse instrumentation in this region missing the phenomena completely, or it may be caused by the expansion of the forebody boundary layer in the shoulder region effectively canceling the local geometric expansion.

The effect of the cowl shock positioning on the inlet performance was determined using a control volume approach. The measured pressure and heat transfer distributions were

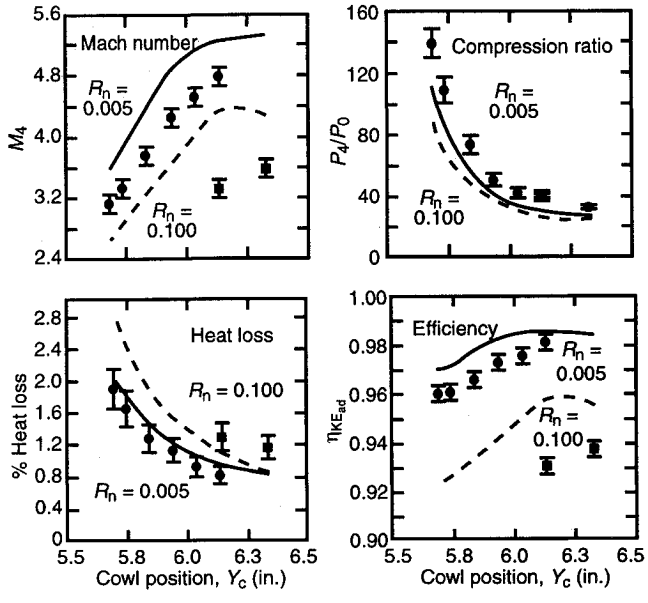

Fig. 11 Comparison of test results and PNS calculations for inlet operation at M_0 = 10.4, Re = 5.7 × 10⁶/ft, and T_w/T_0 = 6.1.

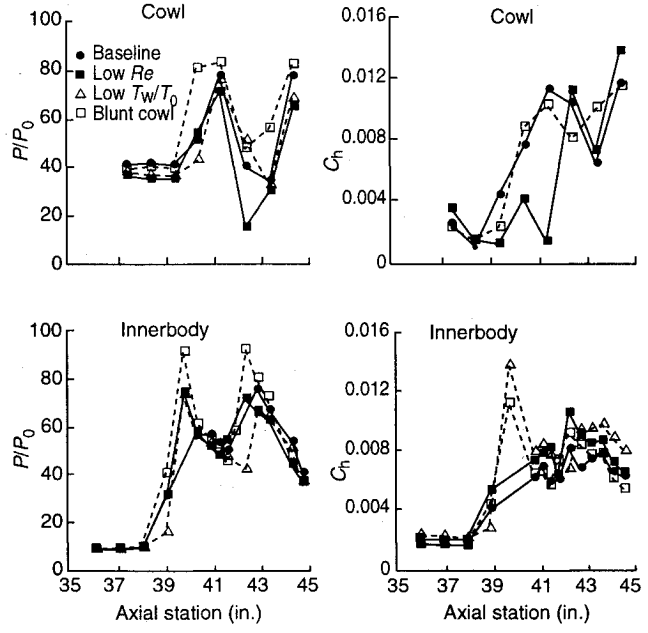

Fig. 12 Effects of Re, T_w/T_0, and R_c on the innerbody and cowl pressure and Stanton number distributions at Y_c = 5.94 in.

used to estimate the drag and heat loss on the portions of the inlet model wetted by the captured airstream. These results were combined with the PNS prediction of the inlet air capture ratio to determine the mass flow, stream thrust, and energy flow at the inlet throat.[12] A one-dimensional set of flow quantities that preserves the mass flow, stream thrust, and energy flow can be determined and is referred to as the set of stream-thrust-averaged flow quantities. The inlet efficiency calculated in this manner generally represents a lower bound on efficiency because the assumption is made that the flow is completely mixed to a uniform state.

Comparisons of the PNS calculations and test results for the deduced inlet operating characteristics are shown in Fig. 11. Comparisons of the stream-thrust-averaged Mach number, compression ratio, and adiabatic kinetic energy efficiency are shown together with the percent heat loss from the captured airstream. The error bars on the data represent the estimated

Table 1 Summary of test conditions

Condition	M_0	Re/ft	T_w/T_0	R_n, in.	R_c, in.
Baseline	10.39	5.7 × 10⁶	6.1	0.005	0.005
Blunt forebody	10.39	5.7 × 10⁶	6.1	0.100	0.005
Blunt cowl	10.39	5.7 × 10⁶	6.1	0.005	0.020
Low Re	10.22	2.2 × 10⁶	6.1	0.005	0.005
Low T_w/T_0	9.89	1.9 × 10⁶	3.0	0.005	0.005

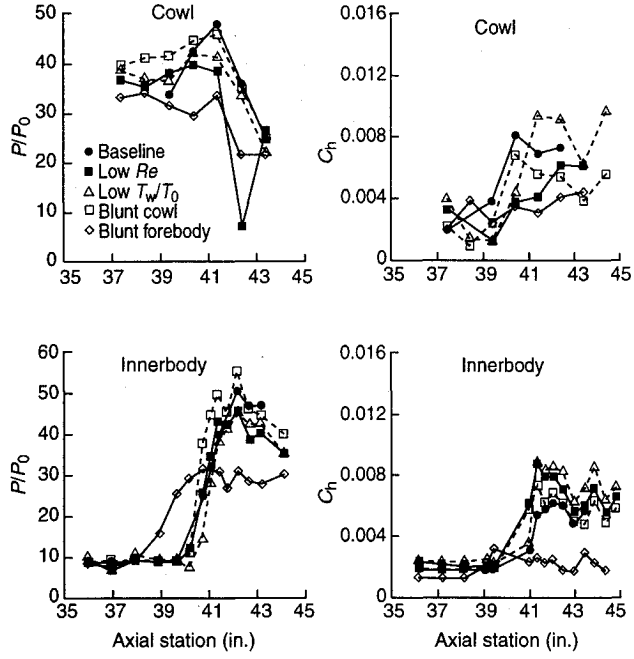

Fig. 13 Effects of Re, T_w/T_0, R_n, and R_c on the innerbody and cowl pressure and Stanton number distributions at Y_c = 6.34 in.

uncertainty in the operating characteristics due to accumulated measurement uncertainties. The results show that M_4 varies between 4.7–2.9, indicating supersonic flow existed in the throat for all test conditions. The test results also show that the $\eta_{KE\text{-}ad}$ for tests with R_n = 0.005 in. varied between 0.981 for operation near the shock-on-shoulder condition to 0.961 for the most contracted operating condition. The uncertainty in inlet efficiency is approximately 0.3%. The results show that the PNS analysis overpredicts the inlet efficiency from 0.3% near the shock-on-shoulder condition up to 1% for the highest contraction case. This overprediction of the inlet efficiency is a direct result of the underprediction of the pressure on the forward forebody ramp and the incorrect prediction of the cowl shock impingement location.

The effect of nose bluntness on the inlet performance can be seen in Fig. 11 by comparing results with R_n = 0.005 and 0.100 in. In the test data, the effect of nose bluntness is to decrease the inlet efficiency by approximately 4–5%. This decrease in inlet performance is caused by the thick entropy layer generated by the blunt nose, which is swallowed by the inlet. The entropy layer also displaces the shock layer outward such that the inlet air capture ratio is significantly reduced. The PNS calculations show the same trends, but the decrement in inlet efficiency is not accurately predicted. The difference between the test data and PNS results is again thought to be caused by the downstream prediction of the cowl shock impingement location.

For cowl heights of 5.94 and 6.34 in., tests were conducted to assess the sensitivity of the inlet operation to R_n, R_c, T_w/T_0, and Re. The conditions evaluated are provided in Table 1. The measured pressure and Stanton number distributions on the innerbody and cowl are provided in Figs. 12 and 13 for Y_c =

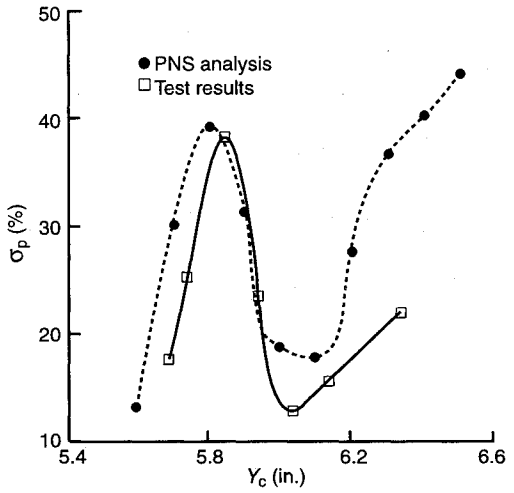

Fig. 14 Effect of cowl height on the measured and calculated wall pressure deviation.

5.94 and 6.34 in., respectively. The results show a significant effect of R_n on the internal flowfield. Changes in Re, R_c, or T_w/T_0 appeared to have only a small effect on the inlet operation with the position of the cowl shock impingement on the innerbody changing approximately 0.5 in. (i.e., approximately one duct height) for the range of variation investigated. Changes to these parameters did affect the location of transition on the cowl, but the density of heat transfer measurements in this region was not adequate to completely define these variations.

As stated previously, a stream-thrust-averaged value of efficiency represents a lower bound on the inlet efficiency since the assumption is made that the inlet throat flow is mixed to a uniform state. Because the entropy increase caused by mixing can be significant, it is desirable to obtain some indication of the increment in inlet efficiency caused by the flow nonuniformity at the inlet throat. The use of the pressure distribution in the constant area section downstream of the inlet throat was investigated for use in inferring information on the throat flow nonuniformity. As can be seen in pressure distributions shown in Figs. 9 and 10, cowl positions that place the cowl shock impingement near the shoulder result in a relatively uniform static pressure throughout the constant area throat. For cowl positions that generate shock impingement either upstream or downstream of the shoulder, the pressure varies widely along the length of the constant area section. A measure of the nonuniformity of this pressure distribution can provide an indication of the flow uniformity at the inlet throat. The area-weighted mean P_{av} and standard deviation σ_p of the pressure distribution on the cowl and innerbody in the constant area throat were calculated for the PNS results as a function of cowl position as follows:

$$P_{av} = \frac{1}{5}\int_{40}^{45} \frac{P_b + P_c}{2}\,dx$$

$$\sigma_p = \left[\frac{1}{5}\int_{40}^{45} \frac{(P_b - P_{av})^2 + (P_c - P_{av})^2}{2}\,dx\right]^{1/2} \Big/ P_{av}$$

A comparison of σ_p from the PNS analysis and the test results is provided in Fig. 14. For the most open cowl position, σ_p is seen to be large as the cowl shock impinges downstream of the shoulder. As the cowl height is decreased, σ_p decreases and reaches a minimum as the shock-on-shoulder condition is reached. Note that at the shock-on-shoulder condition, a finite value of σ_p exists due to the effect of the forebody boundary layer on the shock impingement. As the cowl is lowered beyond the shock-on-shoulder condition, σ_p increases as the cowl shock impingement location moves forward of the shoulder. For the lowest cowl positions, σ_p again decreases as the second shock-on-shoulder condition is approached.

The standard deviation of the wall pressure provides an indication of the flow nonuniformity in the inlet throat. For complete cowl shock cancellation, the throat flow would be uniform and σ_p would be zero. As the throat flow becomes more nonuniform, stronger waves are passed through the constant area duct and σ_p increases. An attempt was made to correlate σ_p vs the inlet throat nonuniformity. The throat flow nonuniformity was characterized in terms of the difference between the mass-averaged kinetic energy efficiency $\eta_{KE\text{-}ma}$ and the stream-thrust-averaged kinetic energy efficiency $\eta_{KE\text{-}sa}$. Because $\eta_{KE\text{-}sa}$ assumes the flow is fully mixed, this difference is representative of the nonuniformity in the inlet throat. If the flow is uniform, $\eta_{KE\text{-}ma} = \eta_{KE\text{-}sa}$. As the flow becomes more nonuniform, $\eta_{KE\text{-}ma}$ becomes larger than $\eta_{KE\text{-}sa}$.

The relationship between σ_p and $(\eta_{KE\text{-}ma} - \eta_{KE\text{-}sa})$ is shown in Fig. 15 for results generated with the PNS codes. Both σ_p and $(\eta_{KE\text{-}ma} - \eta_{KE\text{-}sa})$ exhibit the same trends with changes in the cowl vertical position. The PNS results indicate that at the first shock-on-shoulder condition $(\eta_{KE\text{-}ma} - \eta_{KE\text{-}sa}) = 0.0032$, while $\sigma_p = 20\%$. Applying this same factor to the experimental value of $\sigma_p = 13\%$ would imply an approximate value of $(\eta_{KE\text{-}ma} - \eta_{KE\text{-}sa}) = 0.0021$. This difference between the mass-averaged and stream-thrust-averaged efficiencies can have a significant effect on the engine performance, so it is desirable to have a technique for assessing the flow nonuniformity. Because σ_p is relatively easy to measure in a test, the use of an analytically derived relationship between σ_p and $(\eta_{KE\text{-}ma} - \eta_{KE\text{-}sa})$ allows some information to be determined concerning

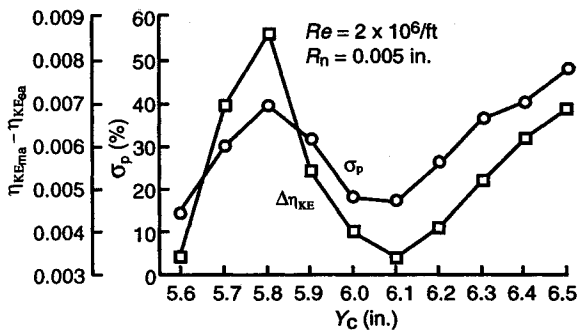

Fig. 15 Correlation of wall pressure deviation and throat flow nonuniformity as calculated with PNS analysis.

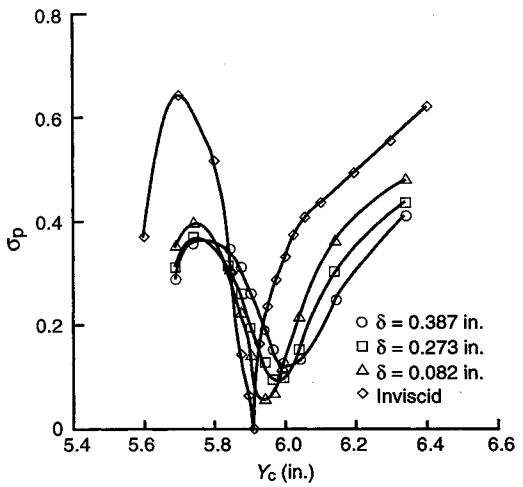

Fig. 16 Effect of forebody boundary-layer thickness on the wall pressure deviation.

the throat flow nonuniformity. If additional accuracy is desired beyond that achieved with this simplified approach, a more refined correlation between σ_p and $(\eta_{\text{KE-ma}} - \eta_{\text{KE-sa}})$ could be generated using a full Navier–Stokes code.

The ability to cancel the cowl shock wave on the innerbody shoulder was investigated numerically using the concept of the wall pressure deviation. By varying the transition location on the forebody, the thickness of the boundary layer at the cowl lip plane could be varied, and the sensitivity of the shock-on-shoulder condition to δ could be assessed. In Fig. 16, the effect of cowl position on σ_p is shown for a range of boundary-layer thicknesses. In this figure, δ is defined as the point where the total enthalpy is equal to 99% of the freestream total enthalpy. The results show that the minimum value of σ_p decreases as δ decreases. In addition, the results indicate that the shape of the curve becomes broader near the minimum as δ increases, indicating the boundary layer smears the interaction near the shoulder.

Conclusions

Comparison of experimental measurements and analytical predictions for the flowfield characteristics in the internal portion of a two-dimensional inlet indicates that the major features of the inlet flowfield are dominated by two-dimensional effects. Although three-dimensional aspects of the inlet flowfield exist, they do not appear to significantly influence the inlet operation.

The control of the positioning of the strong cowl shock within the inlet is a dominant issue in the design of the two-dimensional inlet investigated. The positioning of this shock relative to an innerbody shoulder was shown to significantly influence the inlet efficiency and uniformity of the flow being supplied to a combustor. The effective cancellation of the cowl shock at the innerbody shoulder was demonstrated, despite the effects of the thick forebody boundary layer.

Test results indicate that the effects of Reynolds number, wall-to-freestream temperature ratio, and cowl lip bluntness on inlet operation were minimal over the range of conditions tested. The factors that had a major influence on inlet operation were cowl position and forebody nose bluntness.

The variation of wall pressure in a constant area duct downstream of the inlet throat was shown to be indicative of the flow uniformity in the inlet throat. Because the wall pressure variation is easy to measure in a test, this technique offers an easy method for inferring information concerning the throat flow nonuniformity.

References

[1]Marquart, E. J., "Predictions and Measurements of Internal and External Flowfields of a Generic Hypersonic Inlet," AIAA Paper 91-3320, Sept. 1991.

[2]Seebaugh, W. E., Doran, R. W., and DeCarlo, J. P., "Detailed Investigation of Flowfields with Large Scale Hypersonic Inlet Models," NASA CR-114305, April 1971.

[3]Trexler, C. A., "Inlet Performance of the Integrated Langley Scramjet Module," AIAA Paper 75-1212, Sept. 1975.

[4]Trexler, C. A., and Sanders, S. W., "Design and Performance at a Local Mach Number of 6 of an Inlet for an Integrated Scramjet Concept," NASA TN-D-7944, Aug. 1977.

[5]Torrence, M. G., "Experimental Investigation of a Mach 6 Fixed Geometry Inlet Featuring Swept External-Internal Compression Flowfield," NASA TN-D-7998, Oct. 1975.

[6]Keirsey, J. L., "A Study of the Aerodynamics of Scramjet Engine Inlets," Johns Hopkins Univ., Applied Physics Lab., APL-TG-732, Laurel, MD, Sept. 1965.

[7]Kutschenreuter, P. H., and Balent, R. L., "Hypersonic Inlet Performance from Direct Force Measurements," *Journal of Spacecraft*, Vol. 2, No. 20, 1965, pp. 192–199.

[8]Lai, H. T., Kim, H. T., and Nagamatsu, H. T., "Calculation of Scramjet Inlet with Thick Boundary Layer Ingestion," AIAA Paper 93-1836, June 1993.

[9]Minucci, M. A. S., and Nagamatsu, H. T., "Experimental Studies of a Two-Dimensional Scramjet Inlet, $M_\infty = 10.1–25.1$," *Journal of Propulsion and Power*, Vol. 8, No. 3, 1992, pp. 680–686.

[10]Krawczyk, W. J., and Harris, T. B., "Computational Models for the Analysis/Design of Hypersonic Scramjet Components," AIAA Paper 86-1596, June 1986.

[11]Ault, D. A., and Van Wie, D. M., "Comparison of Experimental Results and Computational Analysis for the External Flowfield of a Scramjet Inlet at Mach 10 and 13," AIAA Paper 92-5100, Dec. 1992.

[12]Van Wie, D. M., "Techniques for the Measurement of Scramjet Inlet Performance at Hypersonic Speeds," AIAA Paper 92-5104, Dec. 1992.